ELSEVIER

Journal of Quantitative Spectroscopy & Radiative Transfer 106 (2007) 21–32

Journal of Quantitative Spectroscopy & Radiative Transfer

www.elsevier.com/locate/jqsrt

Diffuse and coherent backscattering of polarized light: Polarization ratios for a discrete random medium composed of nonspherical particles

Janna M. Dlugach[a], Michael I. Mishchenko[b,*]

[a]*Main Astronomical Observatory of the National Academy of Sciences of Ukraine, 27 Zabolotny Str., 03680, Kyiv, Ukraine*
[b]*NASA Goddard Institute for Space Studies, 2880 Broadway, New York, NY 10025, USA*

Abstract

For a sparse, disordered, plane-parallel particulate medium, we analyze quantitatively the effects of particle microphysical properties on the values of the linear and circular backscattering polarization ratios. Using numerically exact *T*-matrix and vector radiative-transfer codes, we performed computations for the following models: (1) a semi-infinite homogeneous layer composed of randomly oriented, polydisperse oblate spheroids with the real part of the refractive index equal to 1.2, 1.4 and 1.6 and the imaginary part of the refractive index equal to 0 and 0.01; (2) a semi-infinite homogeneous layer composed of randomly oriented, polydisperse, oblate circular cylinders with the refractive index 1.4; (3) finite homogeneous layers of various optical thickness composed of randomly oriented, polydisperse, oblate spheroids with the refractive index 1.55. Our computations demonstrate that the values of the polarization ratios depend substantially on particle shape, real and imaginary parts of the particle refractive index, particle size relative to the wavelength, illumination geometry and optical thickness.

Keywords: Multiple-scattering; Coherent backscattering; Radiative transfer; Polarization; Nonspherical particles

1. Introduction

In this paper, we continue the analysis of the effects of particle properties on the characteristics of coherent backscattering in situations when the incident light is linearly or circularly polarized [1,2]. The interest in these polarization states of the incident light stems from the fact that they are often encountered in practice, e.g. in radar and lidar remote sensing. The results of such observations of particulate media are inevitably affected by coherent backscattering [3–5], and the observed characteristics of light reflected in the exact backscattering direction can yield essential information on the particle microphysical properties. It is, thus, important to analyze theoretically how the observable characteristics of coherent backscattering can be affected by the properties of particles forming a medium, in particular, by particle shape.

*Corresponding author. Tel.: +1 212 678 5590; fax: +1 212 678 5622.
E-mail address: crmim@giss.nasa.gov (M.I. Mishchenko).

0022-4073/$ - see front matter
doi:10.1016/j.jqsrt.2007.01.004

Consistent with the above rationale, the purpose of the present paper is to study the properties of such useful observables as the backscattering polarization ratios. Specifically, we present and discuss the results of theoretical computations of the linear and circular polarizations ratios for sparse, disordered, plane-parallel media composed of polydisperse, randomly oriented oblate spheroids and circular cylinders with varying values of the relative refractive index, effective size parameter, and shape parameter.

2. Basic formulae

Let the scattering medium be a plane-parallel slab composed of randomly distributed, independently scattering particles [6]. The slab is illuminated by a parallel beam of light incident in the direction $\{\theta_0 \geqslant \pi/2, \varphi_0 = 0\}$, where we use the standard radiative-transfer terminology and notation [6,7]. The Stokes vector is defined as a four-component column having the Stokes parameters as its components ($I = [I\,Q\,U\,V]^{\mathrm{T}}$, where T stands for "transposed"), and $\boldsymbol{R}$ is the Stokes reflection matrix for exactly the backscattering direction $\{\theta = \pi - \theta_0,\ \varphi = \pi\}$. Under the assumption of a macroscopically isotropic and mirror-symmetric particulate medium, the matrix $\boldsymbol{R}$ has the following block-diagonal structure [6]:

$$\boldsymbol{R} = \begin{bmatrix} R_{11} & R_{12} & 0 & 0 \\ R_{12} & R_{22} & 0 & 0 \\ 0 & 0 & R_{33} & R_{34} \\ 0 & 0 & -R_{34} & R_{44} \end{bmatrix}. \tag{1}$$

In accordance with the theory of coherent backscattering [6], the matrix $\boldsymbol{R}$ may be decomposed as follows:

$$\boldsymbol{R} = \boldsymbol{R}^{1} + \boldsymbol{R}^{\mathrm{M}} + \boldsymbol{R}^{\mathrm{C}}, \tag{2}$$

where $\boldsymbol{R}^{1}$ is the contribution of the first-order scattering, $\boldsymbol{R}^{\mathrm{M}}$ is the diffuse multiple-scattering contribution consisting of all the ladder diagrams of orders $n \geqslant 2$ and $\boldsymbol{R}^{\mathrm{C}}$ is the cumulative contribution of all the cyclical diagrams. The matrices $\boldsymbol{R}^{1}$ and $\boldsymbol{R}^{\mathrm{M}}$ can be found by solving the full vector form of the radiative transfer equation (see, e.g. [6,7]). Then the matrix $\boldsymbol{R}^{\mathrm{C}}$ can be obtained from the exact relations derived in [8].

In the case of incident light linearly polarized in the vertical direction ($\boldsymbol{I}_0 = [I_0\ I_0\ 0\ 0]^{\mathrm{T}}$), the vertically and horizontally polarized components of the backscattered light are given, respectively, by

$$\tilde{I}_{\mathrm{v}} = \tfrac{1}{2}(\tilde{I} + \tilde{Q}), \tag{3}$$

$$\tilde{I}_{\mathrm{h}} = \tfrac{1}{2}(\tilde{I} - \tilde{Q}), \tag{4}$$

where the tilde is used to denote quantities having the dimension of specific intensity [6]. The linear polarization ratio μ_{L} and its diffuse counterpart $\mu_{\mathrm{L}}^{\mathrm{diff}}$, defined as the ratios of the corresponding cross-polarized and co-polarized backscattered specific intensities, are given by the following formulae:

$$\mu_{\mathrm{L}} = \frac{\tilde{I}_{\mathrm{h}}}{\tilde{I}_{\mathrm{v}}} = \frac{R_{11}^{1} - R_{22}^{1} + R_{11}^{\mathrm{M}} - R_{22}^{\mathrm{M}} - R_{33}^{\mathrm{M}} + R_{44}^{\mathrm{M}}}{R_{11}^{1} + R_{22}^{1} + 2R_{11}^{\mathrm{M}} + 4R_{12}^{\mathrm{M}} + 2R_{22}^{\mathrm{M}}}, \tag{5}$$

$$\mu_{\mathrm{L}}^{\mathrm{diff}} = \frac{\tilde{I}_{\mathrm{h}}^{\mathrm{diff}}}{\tilde{I}_{\mathrm{v}}^{\mathrm{diff}}} = \frac{R_{11}^{1} - R_{22}^{1} + R_{11}^{\mathrm{M}} - R_{22}^{\mathrm{M}}}{R_{11}^{1} + R_{22}^{1} + R_{11}^{\mathrm{M}} + 2R_{12}^{\mathrm{M}} + R_{22}^{\mathrm{M}}}. \tag{6}$$

When the incident light is circularly polarized in the anti-clockwise sense as viewed by an observer looking in the direction of propagation ($\boldsymbol{I}_0 = [I_0\ 0\ 0\ I_0]^{\mathrm{T}}$), the "same-helicity" and "opposite-helicity" components of the backscattered light are given by

$$\tilde{I}_{\mathrm{sh}} = \tfrac{1}{2}(\tilde{I} + \tilde{V}), \tag{7}$$

$$\tilde{I}_{\mathrm{oh}} = \tfrac{1}{2}(\tilde{I} - \tilde{V}). \tag{8}$$

The circular polarization ratio μ_C and its diffuse counterpart μ_C^{diff}, defined as the ratios of the corresponding same-helicity and opposite-helicity backscattered specific intensities, can be found from

$$\mu_C = \frac{\tilde{I}_{sh}}{\tilde{I}_{oh}} = \frac{R_{11}^1 + R_{44}^1 + 2R_{11}^M + 2R_{44}^M}{R_{11}^1 - R_{44}^1 + R_{11}^M + R_{22}^M - R_{33}^M - R_{44}^M}, \tag{9}$$

$$\mu_C^{diff} = \frac{\tilde{I}_{sh}^{diff}}{\tilde{I}_{oh}^{diff}} = \frac{R_{11}^1 + R_{44}^1 + R_{11}^M + R_{44}^M}{R_{11}^1 - R_{44}^1 + R_{11}^M - R_{44}^M}. \tag{10}$$

For grazing incidence and/or a small single-scattering albedo ϖ, the main contribution to the backscattered diffuse radiation comes from the singly scattered light. This means that with $\mu_0 \to 0$ and/or with $\varpi \to 0$ the diffuse multiple-scattering component of the Stokes reflection matrix R^M decreases and ultimately vanishes in comparison with the first-order-scattering component, and from Eqs. (5)–(6) and (9)–(10) we derive

$$\lim_{\mu_0 \to 0} \mu_L = \lim_{\mu_0 \to 0} \mu_L^{diff} = \lim_{\varpi \to 0} \mu_L = \lim_{\varpi \to 0} \mu_L^{diff} = \frac{R_{11}^1 - R_{22}^1}{R_{11}^1 + R_{22}^1} = \delta_L, \tag{11}$$

$$\lim_{\mu_0 \to 0} \mu_C = \lim_{\mu_0 \to 0} \mu_C^{diff} = \lim_{\varpi \to 0} \mu_C = \lim_{\varpi \to 0} \mu_C^{diff} = \frac{R_{11}^1 + R_{44}^1}{R_{11}^1 - R_{44}^1} = \delta_C, \tag{12}$$

where δ_L and δ_C are the single-scattering linear and circular backscattering depolarization ratios [1]. The general analytical properties of the polarization ratios for spherical and randomly oriented nonspherical particles have been studied in detail in [6,9]. In particular,

$$\mu_L \geqslant 0, \tag{13}$$

$$\mu_L^{diff} \geqslant 0, \tag{14}$$

$$\mu_C \geqslant 0, \tag{15}$$

$$\mu_C^{diff} \geqslant 0. \tag{16}$$

3. Numerical results and discussion

To study the potential effect of particle nonsphericity on the linear and circular polarization ratios, we have chosen the model of randomly oriented spheroids and finite circular cylinders distributed over surface-equivalent-sphere radii r according to the simple power law:

$$n(r) = \begin{cases} \text{constant} \times r^{-3}, & r_1 \leqslant r \leqslant r_2, \\ 0 & \text{otherwise.} \end{cases} \tag{17}$$

The effective radius and effective variance of the size distribution are defined by

$$r_{eff} = \frac{1}{\langle G \rangle} \int_{r_1}^{r_2} dr n(r) r \pi r^2, \tag{18}$$

$$v_{eff} = \frac{1}{\langle G \rangle r_{eff}^2} \int_{r_1}^{r_2} dr n(r) (r - r_{eff})^2 \pi r^2, \tag{19}$$

respectively, where

$$\langle G \rangle = \int_{r_1}^{r_2} dr n(r) \pi r^2 \tag{20}$$

is the average area of the geometrical projection per particle [10]. The shapes of spheroids and circular cylinders are fully characterized by a shape parameter, E, defined here as the axis ratio a/b for spheroids, where b is the rotational (vertical) semi-axis and a is the horizontal semi-axis, and the diameter-to-length ratio for cylinders. The computations of the linear and circular polarization ratios and their diffuse counterparts have been performed for semi-infinite and finite homogeneous plane-parallel slabs, and below we shall discuss the results obtained for both cases.

3.1. Semi-infinite slabs

We have considered the case of oblate spheroids with the real part of the refractive index $m_R = 1.2$, 1.4, and 1.6, the imaginary part of the refractive index $m_I = 0$ and 0.01, a range of values of the effective size parameter $x_{eff} = 2\pi r_{eff}/\lambda_1$ (λ_1 is the wavelength of the incident light in the surrounding medium), and axis ratios $1 \leqslant E \leqslant 2$. The effective variance of the size distribution was fixed at 0.1. To make our analysis more representative, analogous computations have also been performed for oblate cylinders with the real part of the refractive index $m_R = 1.4$. We have used the FORTRAN T-matrix codes described in [11] and based on the Waterman's T-matrix approach [12] as well as the vector radiative-transfer codes based on the numerical solution of the Ambarzumian's nonlinear integral equation as described in [6,13]. The main results of these computations are shown in the form of surface plots of μ_L, μ_L^{diff}, μ_C, and μ_C^{diff} as functions of the effective size parameter and shape parameter for $\theta_0 = 0$ ($\mu_0 = 1$) and $\theta_0 = 89.5^\circ$ ($\mu_0 = 0.008$), Figs. 1–5. Note that the results of numerous computations of these characteristics for spherical particles have been presented and analyzed in [4,9].

Fig. 1 depicts the calculated dependences of the linear polarization ratios μ_L and μ_L^{diff} for three values of the real part of the refractive index $m_R = 1.2$ (left-hand column), 1.4 (middle column), and 1.6 (right-hand column) and $m_I = 0$. Let us first analyze the behavior of the full linear polarization ratio μ_L in the case of normal incidence ($\mu_0 = 1$). One can see that for $m_R = 1.2$ and 1.4, μ_L is essentially independent of the shape parameter, but for $m_R = 1.6$ and $x_{eff} > 4$, the dependence on E becomes noticeable. It is seen also that μ_L decreases with m_R. These traits are largely caused by a significant increase in the first-order-scattering contribution with increasing m_R and by multiple scattering being a more efficient depolarizing factor than particle nonsphericity.

In the case of grazing incidence ($\mu_0 = 0.008$), the Stokes reflection matrix is dominated by the first-order scattering contribution. As a result, a pronounced dependence of μ_L on the shape parameter develops, especially for $m_R = 1.2$. Interestingly, the linear polarization ratio is a non-monotonous function of the shape parameter only for $m_R = 1.2$. This behavior of μ_L differs from the corresponding behavior of the helicity-preserving enhancement factor [2] which shows a non-monotonous dependence on the axis ratio for $m_R = 1.4$ and 1.6 as well. Note that μ_L is close to zero in a significant range of x_{eff} and E values. This can be explained as follows: in this range of x_{eff} and E, the values of the elements $F_{11}(\pi)$ and $F_{44}(\pi)$ of the single-scattering Stokes matrix (and, therefore, R_{11}^1 and R_{44}^1) are very close, whereas the multiple-scattering contribution to the reflection matrix is very small. Therefore, the numerator on the right-hand side of Eq. (5) tends to zero. Physically, this corresponds to a very weak linear depolarization.

The calculated dependencies of μ_L^{diff} on x_{eff}, E, m_R, and μ_0 (the two bottom rows of panels in Fig. 1) are qualitatively similar to those for μ_L. Let us also note the following. In the case of normal incidence and in the absence of absorption, $\mu_L < \mu_L^{diff}$ for all values of x_{eff}, E, and m_R considered, which means that coherent backscattering weakens the linear polarization ratio (or the degree of linear depolarization of the backscattered light). However, in the case of grazing incidence and small x_{eff} and/or E, one can see that μ_L can be greater than μ_L^{diff}. With increasing shape parameter E in a number of cases, μ_L becomes smaller than μ_L^{diff}, but we could not find a systematic dependence on the values of x_{eff} and m_R.

Fig. 2 depicts the linear polarization ratios μ_L and μ_L^{diff} in the case of absorbing spheroids with the imaginary part of the refractive index $m_I = 0.01$. One can see a somewhat stronger dependence on x_{eff} and E, especially in the case of normal incidence. It is known that the most obvious effect of increasing absorption is to reduce the single-scattering albedo. Hence, the multiple-scattering contribution to the reflection matrix must also decrease, thereby causing smaller values of μ_L and μ_L^{diff} and stronger dependence on E compared with the case of nonabsorbing particles. Note that our computations exhibit such a decrease in μ_L^{diff} for all values of x_{eff} and m_R considered. As to μ_L, it does decrease with increasing absorption when $m_R = 1.2$. However, in the case of

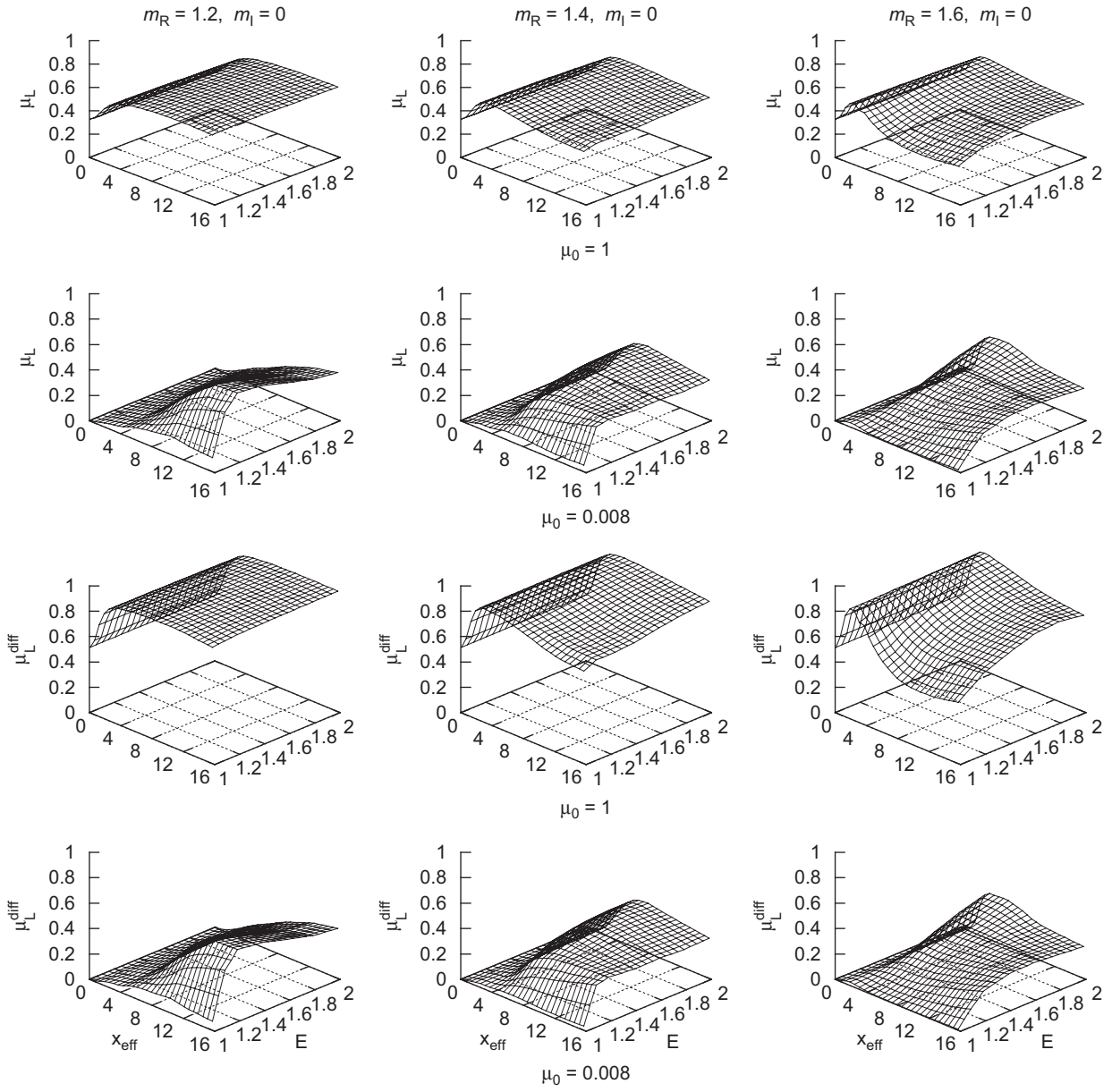

Fig. 1. Polarization ratios μ_L and μ_L^{diff} versus effective equal-surface-area-sphere size parameter x_{eff} and shape parameter E for $m_R = 1.2$, 1.4, and 1.6 and $\mu_0 = 1$ and 0.008. The imaginary part of the refractive index is $m_I = 0$.

normal incidence and $m_R = 1.4$ and 1.6, the full polarization ratio can increase with m_I. This kind of behavior of μ_L in the case of spherical particles was discussed in [9] and was attributed to the extreme complexity of the process of multiple scattering. Note that for grazing incidence, the increase of μ_L with m_I is hardly noticeable because of the much reduced multiple-scattering contribution to the reflection matrix. It is also worth noticing that unlike the case of nonabsorbing spheroids, $\mu_L|_{\mu_0=1}$ can be greater than $\mu_L^{diff}|_{\mu_0=1}$ for certain values of x_{eff} and E and for all values of m_R considered.

Fig. 3 is similar to Fig. 1 but shows the results of computations of the circular polarization ratios μ_C and μ_C^{diff} for $m_R = 1.2$, 1.4, and 1.6 and $m_I = 0$. One can see that in the case of normal incidence and $m_R = 1.6$ and 1.4, the dependence of μ_C on E is stronger than that of μ_L. This is also true of the dependence on x_{eff} for all

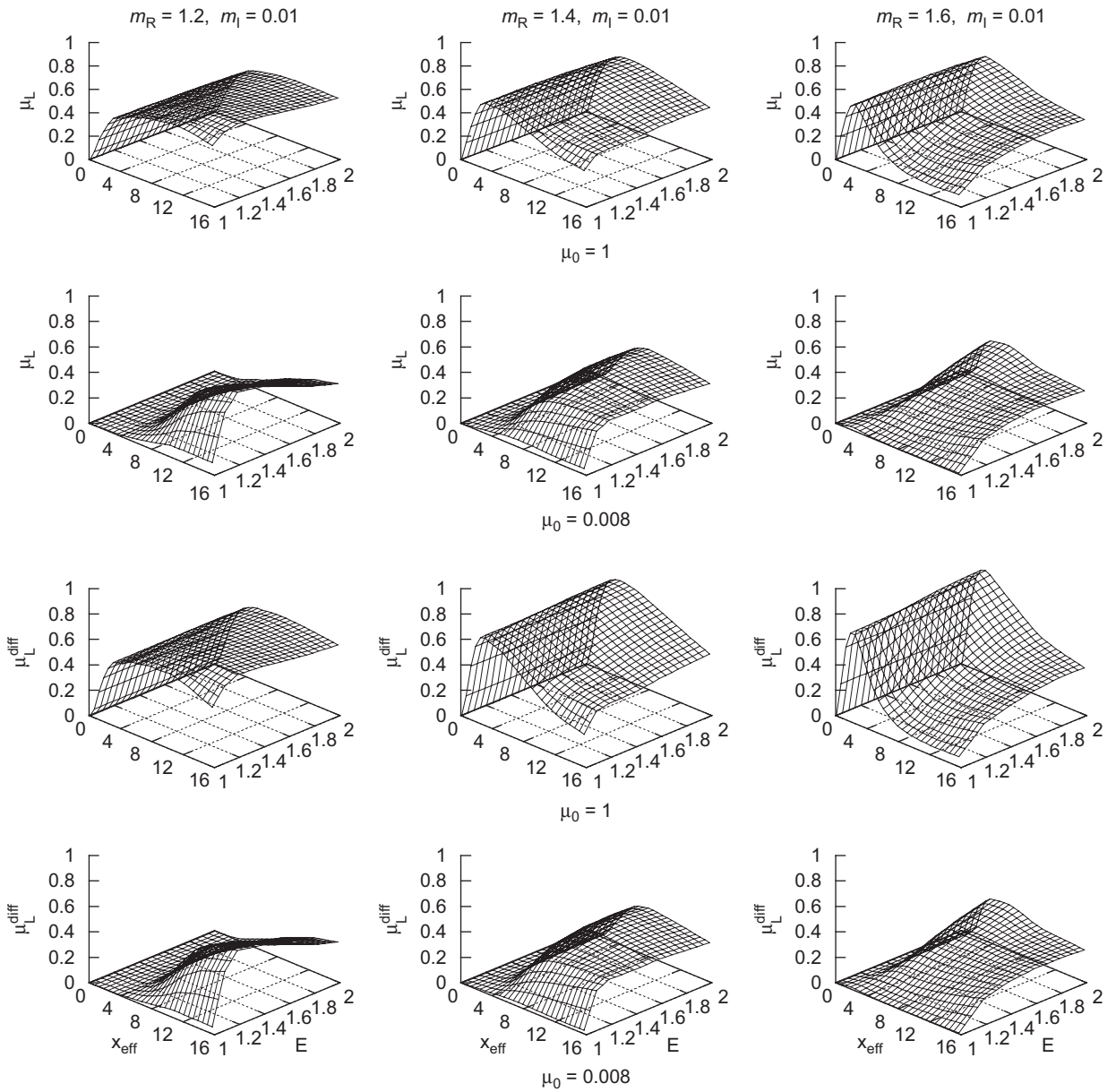

Fig. 2. Polarization ratios μ_L and μ_L^{diff} versus effective equal-surface-area-sphere size parameter x_{eff} and shape parameter E for $m_R = 1.2$, 1.4, and 1.6 and $\mu_0 = 1$ and 0.008. The imaginary part of the refractive index is $m_I = 0.01$.

three values of m_R considered. In the case of grazing incidence, the calculated dependences of μ_C are qualitatively similar to those for μ_L, but show much greater μ_C values.

The effect of absorption ($m_I = 0.01$) on the behavior of the circular polarization ratios is illustrated by Fig. 4. In comparison with the respective linear polarization ratios, the dependence of μ_C and μ_C^{diff} on x_{eff} and E is more pronounced, especially in the case of normal incidence. The diagrams for μ_C and μ_C^{diff} are qualitatively more similar to each other than the corresponding diagrams for the linear polarization ratios. In particular, for $m_R = 1.4$ and 1.6 and in the range of small size parameters, μ_C and μ_C^{diff} show almost the same behavior with increasing absorption: they first decrease with increasing absorption, then rapidly increase, and finally decrease again. We remind the reader that in the case of linear polarization, this behavior was found

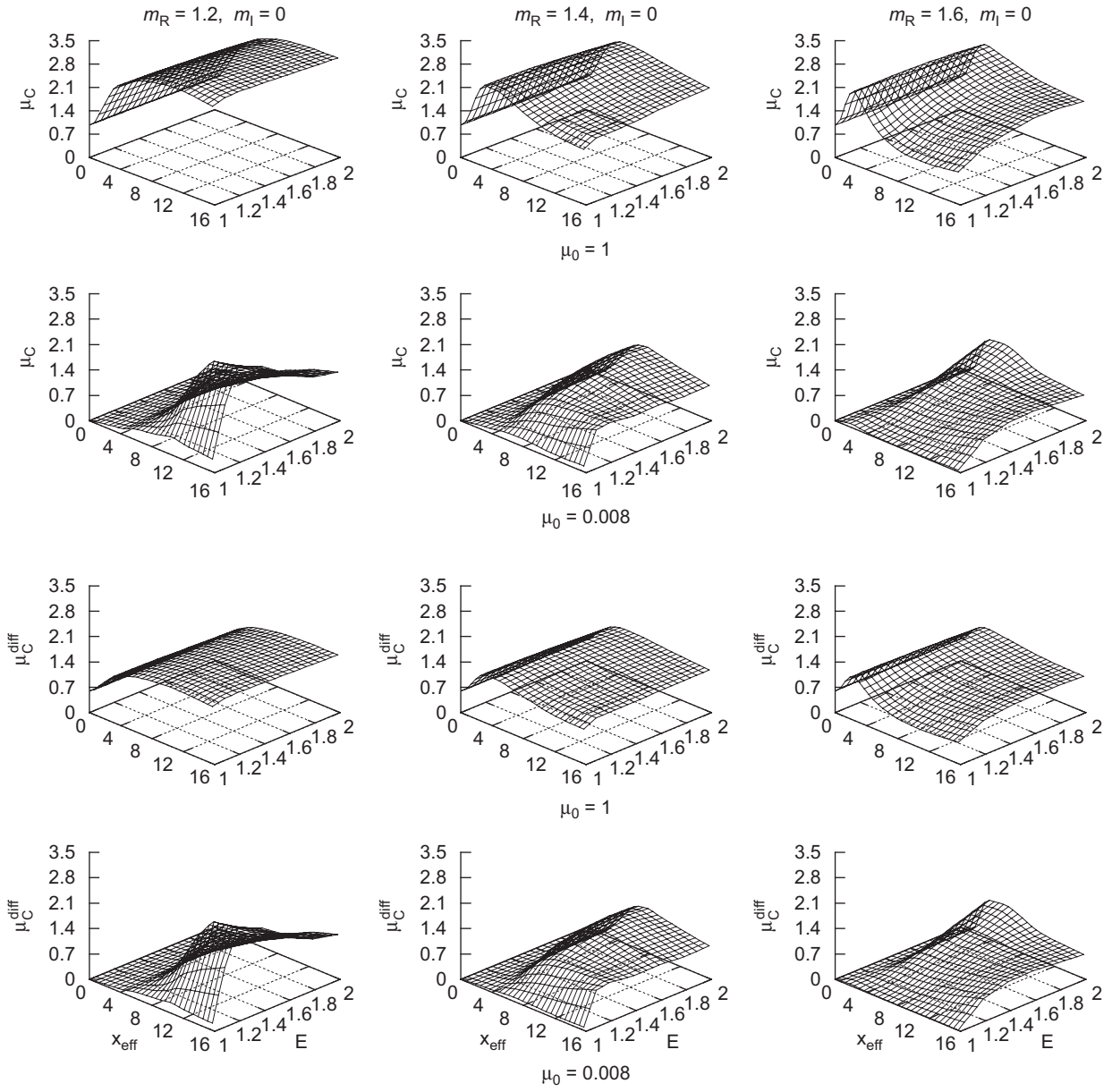

Fig. 3. Polarization ratios μ_C and μ_C^{diff} versus effective equal-surface-area-sphere size parameter x_{eff} and shape parameter E for $m_R = 1.2$, 1.4, and 1.6 and $\mu_0 = 1$ and 0.008. The imaginary part of the refractive index is $m_I = 0$.

only for the full polarization ratio μ_L. It is interesting to note that our computations for $m_R = 1.4$ and 1.6 and $m_I = 0$ and 0.01 show that $\mu_C^{diff} < \mu_C$ for both normal and grazing incidence. However, for $m_R = 1.2$, $m_I = 0.01$ and grazing incidence, $\mu_C^{diff} > \mu_C$ for some values of x_{eff} and E. This result is at variance with the conclusion made in [6,9] that for spherical particles μ_C^{diff} is always smaller than or equal to μ_C, thereby illustrating a different behavior of the helicity preserving and opposite-helisity enhancement factors for spherical and nonspherical particles [2]. In addition we must note again that in many cases, the values of the circular polarization ratios μ_C and μ_C^{diff} are much greater than those of their linear polarization counterparts (cf. [4,9]).

In order to extend the analysis of the effect of particle shape on the polarization ratios, we have also performed computations for a semi-infinite slab composed of polydisperse, randomly oriented, finite circular

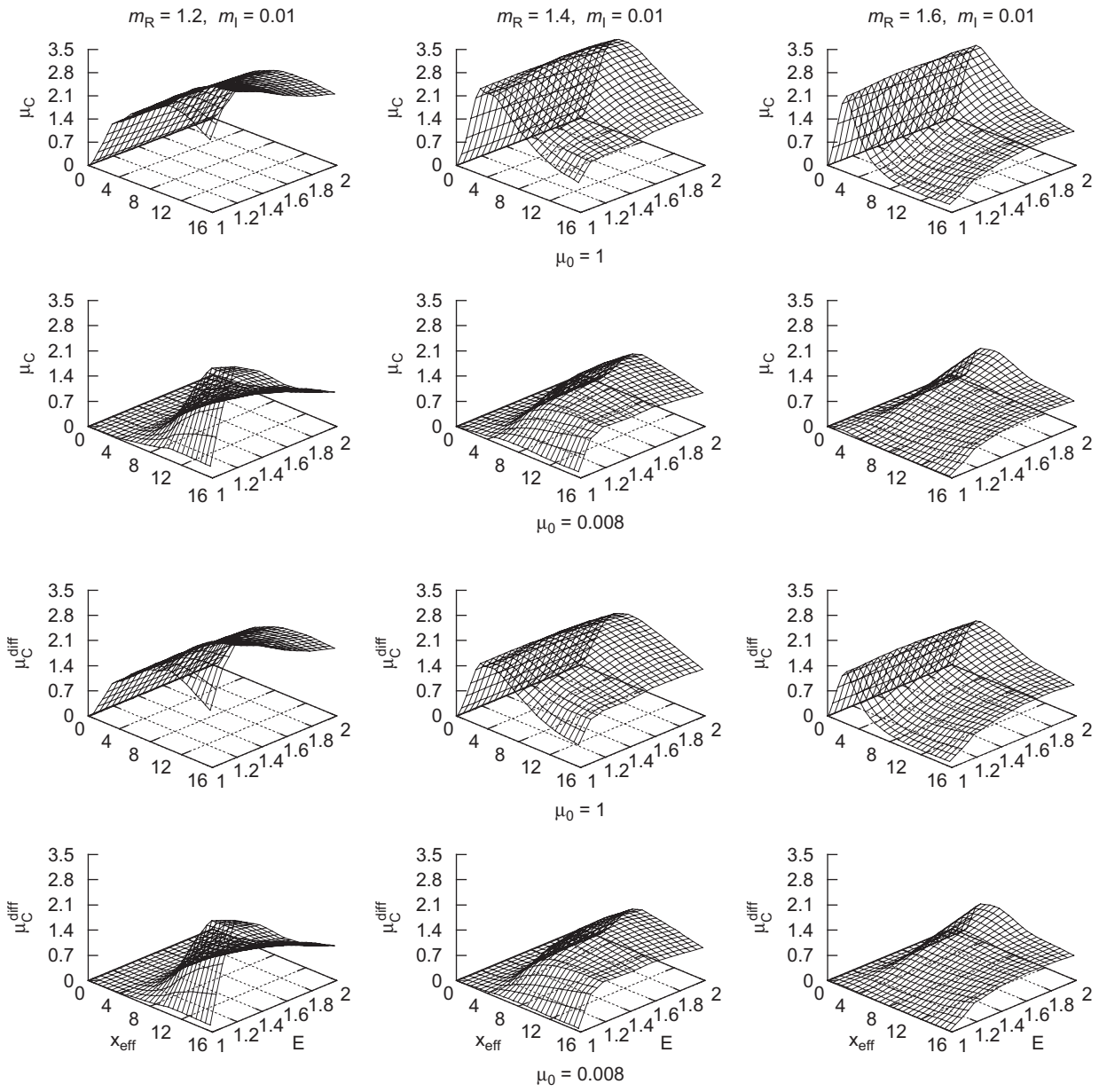

Fig. 4. Polarization ratios μ_C and μ_C^{diff} versus effective equal-surface-area-sphere size parameter x_{eff} and shape parameter E for $m_R = 1.2$, 1.4, and 1.6 and $\mu_0 = 1$ and 0.008. The imaginary part of the refractive index is $m_I = 0.01$.

cylinders with $m_R = 1.4$ and $m_I = 0$ (Fig. 5). It is seen that the ratios μ_L and μ_C for the cylinders can exceed those for the size- and shape-parameter-equivalent spheroids, especially for larger x_{eff}. Overall, the results for the E-equivalent spheroids and cylinders are rather similar.

3.2. Slabs of finite optical thickness

In this subsection, we consider finite plane-parallel particulate slabs with varying optical thickness T. Computations of the linear and circular polarization ratios have been performed for optical thickness values

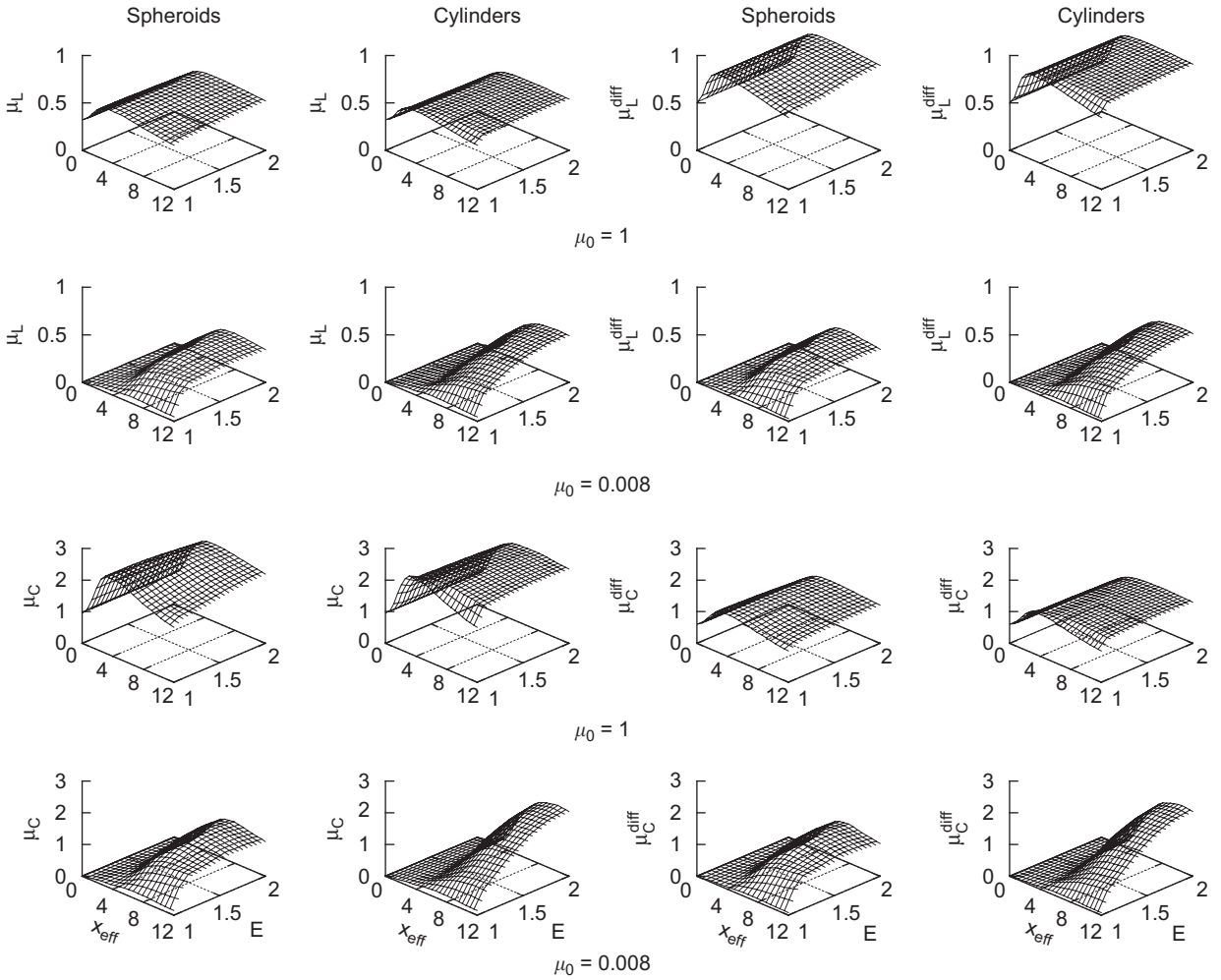

Fig. 5. Polarization ratios μ_L, μ_L^{diff}, μ_C, and μ_C^{diff} versus effective equal-surface-area-sphere size parameter x_{eff} and shape parameter E for oblate spheroids and cylinders with $m_R = 1.4$ and $m_I = 0$.

$T = 0.01$, 0.1, 1, 10 and for layers composed of oblate spheroids with $m_R = 1.55$ and $m_I = 0$. To compute the elements of the matrix $\boldsymbol{R}^M$, we have used a computational algorithm based on the invariant imbedding technique as described in [6,14].

Fig. 6 depicts the calculated dependences of the linear polarization ratios μ_L and μ_L^{diff} on size parameter x_{eff} and shape parameter E for $\mu_0 = 1$ and 0.008. One can see that in the case of normal incidence both μ_L and μ_L^{diff} increase strongly with T. The dependence on the shape parameter E is quite noticeable for small T, but weakens with increasing optical thickness. Besides, for $T = 0.01$, 0.1, and 1 the values of μ_L and μ_L^{diff} are close to each other. This means that the effect of coherent backscattering is rather weak. However, for $T = 10$, analogously to the case of a semi-infinite medium, $\mu_L < \mu_L^{diff}$ for all values of x_{eff} and E considered.

In the case of grazing incidence, there is no strong dependence of μ_L and μ_L^{diff} on T and the μ_L and μ_L^{diff} values are nearly identical. These traits are a direct consequence of the dominance of the first-order-scattering contribution to the Stokes reflection matrix. For the same reason, the dependences of μ_L and μ_L^{diff} on x_{eff} and E are very similar to those found for a semi-infinite layer. Specifically, one can see that both μ_L and μ_L^{diff} vary with shape parameter when $x_{eff} > 4$, and there is a significant range of x_{eff} and E values where both ratios are very close to zero, consistent with Eq. (11).

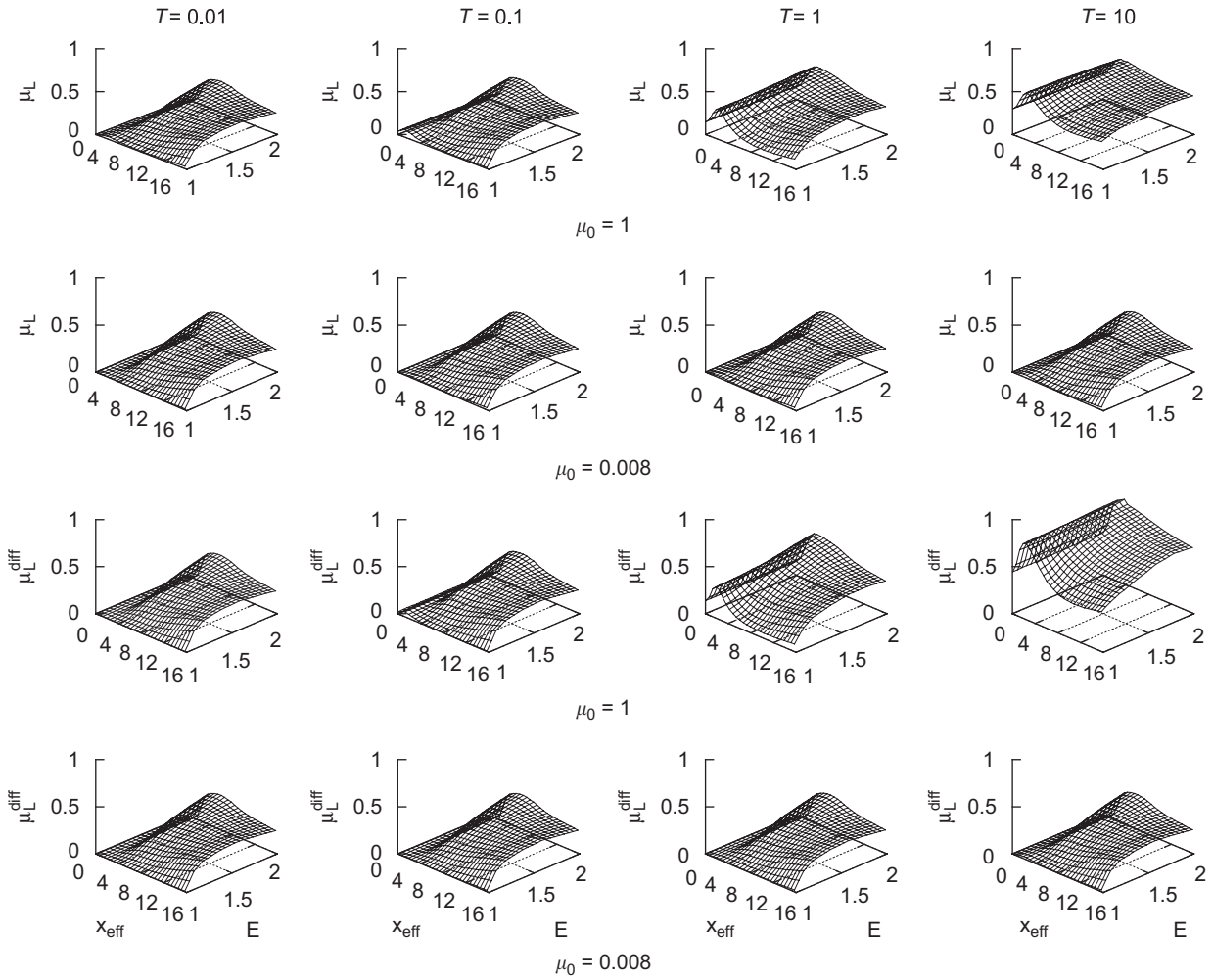

Fig. 6. Polarization ratios μ_L and μ_L^{diff} versus effective equal-surface-area-sphere size parameter x_{eff} and shape parameter E for $T = 0.01$, 0.1, 1, and 10 and $\mu_0 = 1$ and 0.008. The real part of the spheroid refractive index is $m_R = 1.55$ and the imaginary part is $m_I = 0$.

The results of computations of the circular polarization ratio μ_C and its diffuse counterpart μ_C^{diff} for the same optical thickness values are shown in Fig. 7. When $\mu_0 = 1$, one can see that μ_C and μ_C^{diff} are close to each other when $T = 0.01$ and 0.1. Similarly to the case of linear polarization, there is a significant range of x_{eff} and E values where both μ_C and μ_C^{diff} are close to zero. Both μ_C and μ_C^{diff} increase with T, their dependence on E becomes weaker, and μ_C becomes greater than μ_C^{diff}. For grazing incidence, the μ_C and μ_C^{diff} values are close to each other and hardly vary with optical thickness.

4. Conclusions

Using the model of a sparse, disordered, plane-parallel particulate slab composed of randomly oriented oblate spheroids and cylinders, we have demonstrated that the values of the backscattering polarization ratios depend substantially on particle shape, real and imaginary parts of the particle refractive index, particle size, illumination geometry, and optical thickness. The dependence on particle shape is more pronounced in the case of circular polarization, and in many cases the values of the circular polarization ratios are much greater than those of their linear polarization counterparts. These results suggest that laboratory and remote-sensing

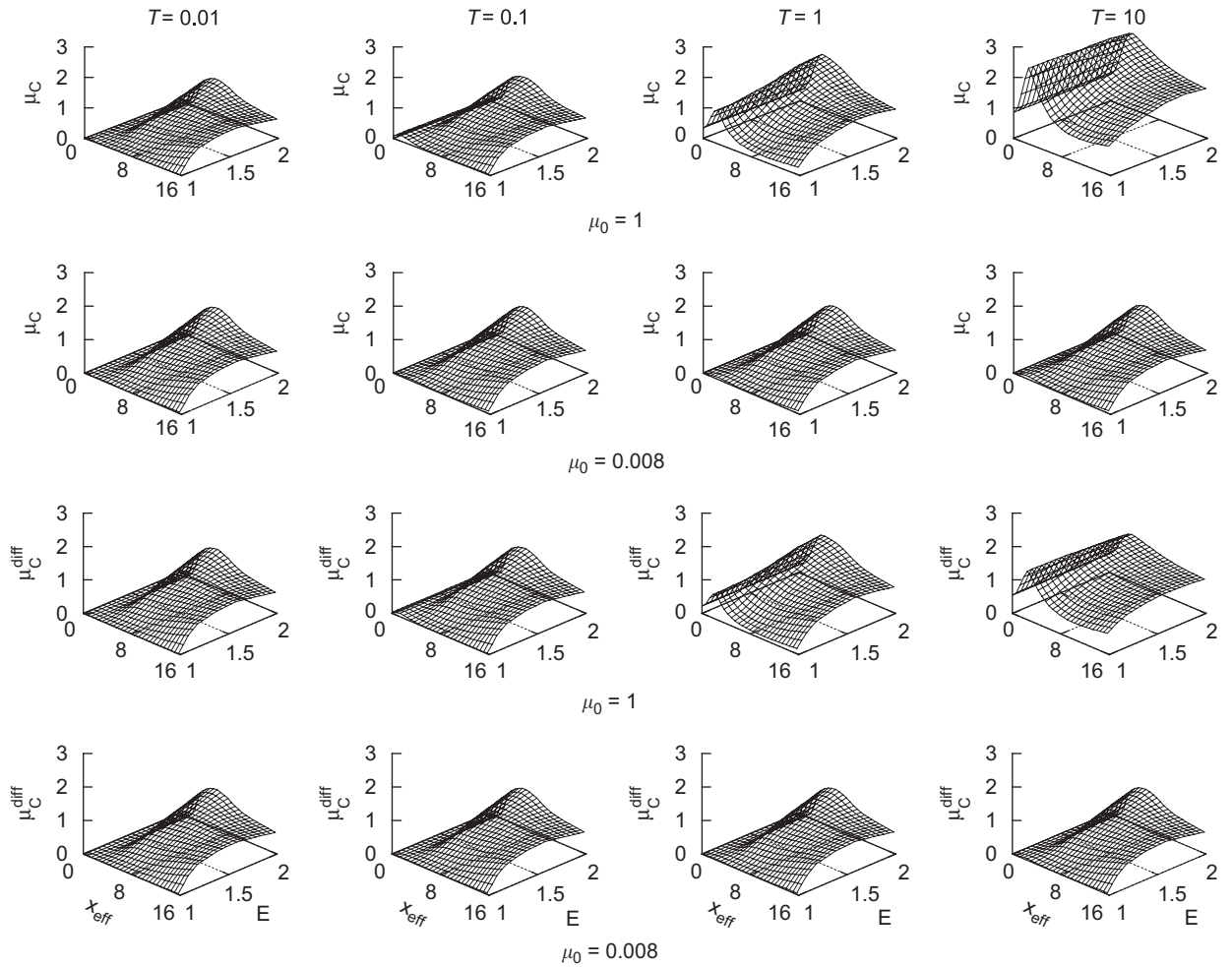

Fig. 7. Polarization ratios μ_C and μ_C^{diff} versus effective equal-surface-area-sphere size parameter x_{eff} and shape parameter E for $T = 0.01$, 0.1, 1, and 10 and $\mu_0 = 1$ and 0.008. The real part of the spheroid refractive index is $m_{\mathrm{R}} = 1.55$ and the imaginary part is $m_{\mathrm{I}} = 0$.

measurements of the linear and circular backscattering polarization ratios can potentially be used as an efficient particle characterization tool.

Acknowledgment

This research was partially supported by the NASA Radiation Sciences Program managed by Hal Maring.

References

[1] Mishchenko MI, Hovenier JW. Depolarization of light backscattered by randomly oriented nonspherical particles. Opt Lett 1995;20:1356–8.
[2] Dlugach JM, Mishchenko MI. Enhanced backscattering of polarized light: effect of particle nonsphericity on the helicity-preserving enhancement factor. JQSRT 2006;100:115–21.
[3] Hapke B. Coherent backscatter and the radar characteristics of outer planet satellites. Icarus 1990;88:407–17.
[4] Mishchenko MI. Polarization characteristics of the coherent backscatter opposition effect. Earth Moon Planets 1992;58:127–44.
[5] Ostro SJ. Planetary radar astronomy. Rev Mod Phys 1993;16:1235–79.
[6] Mishchenko MI, Travis LD, Lacis AA. Multiple scattering of light by particles: radiative transfer and coherent backscattering. Cambridge: Cambridge University Press; 2006.

[7] Hovenier JW, van der Mee C, Domke H. Transfer of polarized light in planetary atmospheres—basic concepts and practical methods. Berlin: Springer; 2004.
[8] Mishchenko MI. Enhanced backscattering of polarized light from discrete random media: calculations in exactly the backscattering direction. J Opt Soc Am A 1992;9:978–82.
[9] Mishchenko MI. Diffuse and coherent backscattering by discrete random media—1. Radar reflectivity, polarization ratios, and enhancement factors for a half-space of polydisperese, nonabsorbing and absorbing spherical particles. JQSRT 1996;56:673–702.
[10] Mishchenko MI, Travis LD, Lacis AA. Scattering, absorption, and emission of light by small particles. Cambridge: Cambridge University Press; 2002 (available in the PDF format at http://www.giss.nasa.gov/~crmim/books.html).
[11] Mishchenko MI, Travis LD. Capabilities and limitations of a current FORTRAN implementation of the *T*-matrix method for randomly oriented rotationally symmetric scatterers. JQSRT 1998;60:309–24.
[12] Waterman PC. Symmetry, unitarity, and geometry in electromagnetic scattering. Phys Rev D 1971;3:825–39.
[13] de Rooij WA. Reflection and transmission of polarized light by planetary atmospheres. PhD dissertation. Amsterdam: Vrije Universiteit; 1985.
[14] Mishchenko MI. The fast invariant imbedding method for polarized light: computational aspects and numerical results for Rayleigh scattering. JQSRT 1990;43:163–71.